Chemical Science

ROYAL SOCIETY OF CHEMISTRY

EDGE ARTICLE

View Article Online
View Journal | View Issue

Cite this: *Chem. Sci.*, 2023, **14**, 331

All publication charges for this article have been paid for by the Royal Society of Chemistry

Received 2nd November 2022
Accepted 28th November 2022

DOI: 10.1039/d2sc06035c

rsc.li/chemical-science

A highly conductive gel electrolyte with favorable ion transfer channels for long-lived zinc–iodine batteries†

Yadong Tian, Song Chen, Siyu Ding, Qianwu Chen and Jintao Zhang *

Aqueous rechargeable zinc–iodine batteries (ARZIBs), as a powerful energy alternative, have inherent advantages, such as low cost, good safety and environmental friendliness. Unfortunately, uneven Zn deposition with dendrite growth and undesirable side reactions seriously compromises the safety and stability of ARZIBs. Herein, a novel strategy is demonstrated to fabricate highly conductive iota-carrageenan (IC) gel electrolyte. The unique double helix structure with good mechanical properties provides favorable Zn^{2+} channels guided by sulfate groups, which enables confinement effect and orderly guidance of Zn deposition. Additionally, the activity of water molecules confined in the gel electrolyte is reduced, thus inhibiting the corrosion reactions of the zinc electrode. As a result, the gel electrolyte with remarkable ionic conductivity (42.95 mS cm^{-1}) showed a good cycling stability over 1000 h. Importantly, the Zn–I_2 batteries with the IC–Zn gel electrolyte demonstrated remarkable reversibility with an impressive capacity retention (91.9%) over 5000 cycles and high average coulombic efficiency (99.86%). This work provides a reliable strategy to develop natural polymer gel electrolytes to regulate the Zn deposition for advanced rechargeable Zn–I_2 batteries.

Introduction

Rechargeable Zn-based batteries with aqueous electrolytes have attracted extensive attention in recent years due to their inherent advantages, such as good safety, large theoretical specific capacity (820 mA h g^{-1}), low cost and environmental friendliness.[1–5] However, free water molecules inevitably result in corrosion of the Zn anode in accord with the Pourbaix diagram.[6] Additionally, the growth of Zn dendrites due to uneven Zn deposition causes potential safety risks and short-lived lifespans.[7–10] Thus, Zn dendrites also complicate the parasitic reactions of the electrolyte, thereby intensifying the production of by-products (*e.g.*, $Zn_4SO_4(OH)_6 \cdot 3H_2O$). Therefore, it is highly desirable to inhibit the growth of Zn dendrites and corrosion for the development of high-performing Zn-based batteries.

Advanced strategies, including anode surface modification,[11,12] electrolyte composition optimization[13,14] and gel electrolytes,[15,16] have been proposed to improve the cycling stability and battery performance. New electrolytes reported in recent years, such as $ZnCl_2$–acetamide[17] and $Zn(TFSI)_2$–LiTFSI,[18] regulate the deposition of Zn to inhibit the growth of dendrites by changing the solvent sheath structure of the Zn ions. Additionally, a small amount of electrolyte additive, such as TMA^+,[13] TBA_2SO_4 (ref. 19) or Et_2O,[20] can also have a significant effect. The preferred adsorption of these huge organic cations/molecules inhibits dendrite growth *via* the charge-shielding effect. However, problems such as electrolyte leakage, frequent hydrogen evolution side reactions and dissolution of electroactive materials are still unavoidable for aqueous electrolytes.[21] Fortunately, gel electrolytes can effectively alleviate these problems.[15] Due to their limited water content, gel electrolytes have natural advantages in resisting water-induced corrosion and dissolution of electroactive materials. Nevertheless, inefficient ion transport increases transfer barriers, leading to slow reaction kinetics. Moreover, gel electrolytes suffer from low ionic conductivity and mild inhibiting effects on Zn dendrites. Currently, the development of a highly conductive gel electrolyte with rapid ion transfer abilities to inhibit Zn dendrite growth remains a formidable challenge.

Iota-carrageenan (IC) is a pure natural polymer compound extracted from red algae and has been widely used in the food industry due to its characteristics of being green, protecting the environment, non-toxic and low cost.[22,23] As a polysaccharide sulfate composed of D-galactose and 3,6-anhydro-D-galactose, the binding ability of IC with cations is equivalent to inorganic sulfates, because of ester sulfates.[22] Herein, an IC–Zn gel was prepared *via* the cold-set mechanism coupled with the cation bridging effect.[22] The cold-set mechanism is a gelation mechanism that refers to the formation of an intermolecular helix to

Key Laboratory for Colloid and Interface Chemistry, Ministry of Education, School of Chemistry and Chemical Engineering, Shandong University, Jinan 250100, China. E-mail: jtzhang@sdu.edu.cn; Fax: +86-531-88361011

† Electronic supplementary information (ESI) available. See DOI: https://doi.org/10.1039/d2sc06035c

achieve gelation on cooling from a hot solution.[22,24] The spontaneously formed double helix structure would provide feasible channels, guided by sulfate groups, to accelerate Zn ion transfer. Subsequently, the uniform ion channels formed would confine and guide orderly Zn deposition for enhancing cycling reversibility. As expected, the symmetrical cells assembled with the IC–Zn gel electrolyte displayed a stable cycling lifespan of over 1000 h, which is ten times longer than that of the aqueous electrolyte (about 100 h). With the help of the IC–Zn gel electrolyte, Zn–I_2 batteries delivered remarkable stability for 5000 cycles with an impressive capacity retention (91.9%). IC–Zn gel electrolyte offers favorable stability and high conductivity to enhance the energy storage performance of rechargeable Zn–I_2 batteries.

Results and discussion

As shown in Fig. 1a, the abundant sulfate groups of IC are combined with Zn^{2+} *via* the bridging effect to constitute the IC–Zn gel electrolyte (Fig. 1b), which demonstrates its favorable flexibility. IC–Zn is a uniform yellowish gel with a thickness of 0.15 mm (Fig. S1†). As shown in Fig. 1c, The sulfate groups of IC are external to the helices, resulting in the negative charge along the individual helix. The electrostatic repulsion is counterbalanced by cooperative hydrogen bond attractions. The physical thermo-reversible gel formed is also stabilized by hydrogen bonds between random double helices.[25,26] After the exchange process, a cross-linking network would be formed through cation bridging of Zn^{2+} to further stabilize the double helix and thus enhance the mechanical properties (Fig. 1d). The polymer chains with sulfate groups provide zinc ion channels *via* cation bridging (Fig. 1e), which are highly promising to enhance the transport of Zn^{2+} ions and to guide orderly and uniform Zn deposition.[27,28] The cross-section images from scanning electron microscopy (SEM) exhibit a layered structure, possibly due to the formation of the double helix structure with a layered arrangement *via* the cold-set mechanism (Fig. S2a†). Elemental mapping images show that the IC gel is composed of C, O and S (Fig. S2b†). The IC–Zn gel electrolyte is filled with uniformly distributed Zn ions compared with the IC gel (Fig. S3†). Traditional aqueous Zn-based batteries with glass fiber (GF) separators suffer from the growth of Zn dendrites due to the tip effect (Fig. 1f).[29,30] Additionally, free water molecules would induce corrosion reactions of Zn, leading to the formation of by-products (*e.g.*, $Zn_4SO_4(OH)_6{\cdot}3H_2O$) with poor electrical conductivity.[31] In contrast, IC–Zn gel electrolyte, with the assistance of ion channels, can effectively regulate the Zn^{2+} flux to inhibit dendrite growth for uniform deposition (Fig. 1g).

In the Fourier-transform infrared (FT-IR) spectrum of IC–Zn, the wide absorption peak at 3243 cm^{-1} is assigned to the O–H stretching vibration of hydrogen bonds in polymer chains (Fig. 2a). The red shift of the absorption peak can be attributed to the enhanced hydrogen bonds compared with IC powder (3363 cm^{-1}). This indicates that the free water molecules from the solvation sheath of Zn^{2+} are trapped by the oxygen-containing functional groups within the polymer chains with ion channels, to form rich hydrogen bonds, thus suppressing the activity of water.[32] The characteristic peaks at 1636 cm^{-1} and 1220 cm^{-1} are ascribed to the C–H asymmetric bending vibrations of $-CH_2-$ groups and the C–O–C stretching vibrations, respectively. The IC powder shows that the characteristic peak at 1034 cm^{-1} is indexed to the sulfated group of S=O.[33] For IC–Zn, the blue shift of the absorption peak at 1074 cm^{-1} can be attributed to the cation bridging effect, in comparison with the IC powder (1034 cm^{-1}). In contrast, no corresponding

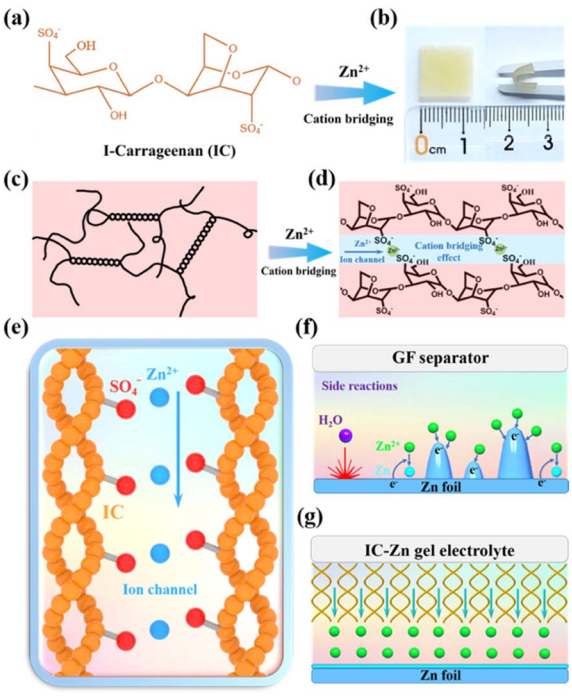

Fig. 1 (a) Chair configuration of iota-carrageenan. (b) Optical photographs of IC–Zn gel electrolyte. The proposed structures of (c) IC gel and (d) IC–Zn gel, respectively. (e) Zinc ion channel in IC–Zn gel electrolyte. Schematic illustrations of the behavior of Zn anodes with (f) $ZnSO_4$ aqueous electrolyte and (g) IC–Zn gel electrolyte in Zn deposition.

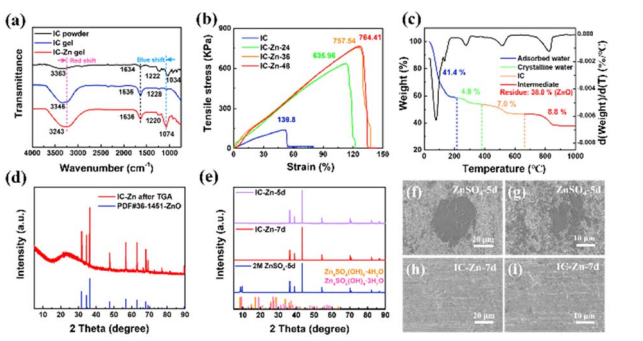

Fig. 2 (a) FT-IR spectra of IC–Zn gel, IC gel and IC powder. (b) Tensile curves of IC–Zn-*T* gel electrolytes with changing ion exchange time (IC–Zn-*T*, *T* = 0 h, 24 h, 36 h, 48 h). (c) TGA curve of IC–Zn gel electrolyte. (d) XRD pattern of IC–Zn after TGA. (e) XRD patterns of Zn foils for corrosion test. SEM images of (f and g) $ZnSO_4$-5 d and (h and i) IC–Zn-7 d (Zn foil soaked in IC–Zn for 7 days).

characteristic peak is observed for the pure IC gel. The results show that the coordination between Zn^{2+} and iota-carrageenan leads to the cation bridging effect.

The mechanical properties of the IC–Zn-*T* gel electrolyte with different ion exchange times (T = 0 h, 24 h, 36 h, 48 h) was evaluated using a universal materials testing machine. As displayed in Fig. 2b, both IC–Zn-36 and IC–Zn-48 exhibited similar tensile strengths of up to 758 and 764 kPa, respectively, with a high strain of 127.6% (Fig. S4†). IC–Zn-24 showed a slightly lower tensile strength (636 kPa) with a strain of 112.6%. In contrast, the tensile strength for IC gel without ion exchange is only 139.8 kPa with a strain of 51.3%. The tensile strength for IC–Zn-36 and IC–Zn-48 is five times more than that of IC gel. Note that the gel properties are highly dependent on the helix formation from blocks of IC and the length of the helices. The superior mechanical properties of IC–Zn-36 and IC–Zn-48 compared to IC gel are attributed to the formation of ion pairs *via* the cation bridging effect between Zn^{2+} and sulfuric acid groups, which would increase helix formation with the cross-linked network and thus greatly improve the mechanical properties and stability of the gel electrolyte. The similar mechanical properties of IC–Zn-36 and IC–Zn-48 indicate that the ion exchange can be achieved in 36 h to obtain optimal tensile strength.

The composition of the IC–Zn gel electrolyte was analysed by thermogravimetric analysis (TGA). As presented in Fig. 2c, the rapid weight loss below 210 °C can be attributed to volatilization of the physically adsorbed water. The slow weight loss between 210 °C and 380 °C is caused by loss of crystalline water.[34] Thus, the water content is about 46.2 wt% in IC–Zn gel. The weight loss between 380 °C and 660 °C was assigned to decomposition of IC. Subsequent decomposition of the organic component gave ZnO with a mass accounting for 38 wt% according to the X-ray diffraction (XRD) results (Fig. 2d). According to the inductively coupled plasma-mass spectrometry (ICP-MS), the content of Zn^{2+} was 126.49 g dm^{-3} in the IC–Zn gel electrolyte, which is equivalent to the content of Zn^{2+} in 2 M $ZnSO_4$ aqueous solution, and which would facilitate rapid ion transmission and ultra-high ionic conductivity. According to the TGA curves, the water content of the IC–Zn-*T* (T = 24, 36, 48) gel electrolytes was 48.9, 46.2 and 47.2 wt%, respectively (Fig. S5†). The results demonstrate that the exchange process does not change the water content of such IC–Zn-*T* electrolytes significantly.

To evaluate the influence of the water content, the mechanical and electrochemical properties of the IC–Zn gel electrolytes with different water content were tested. As shown in Fig. S6,† the IC–Zn gel after dehydration delivered a low strain with a high tensile strength, compared with the initial state, suggesting the formation of a rigid and brittle gel with reduced flexibility after dehydration. Additionally, the ionic conductivity of the IC–Zn gel electrolyte also decreased with decreasing water content (Fig. S7†). Thus, the water content has to be maintained for favorable ion transfer.

In aqueous electrolyte, metal electrodes suffer from unavoidable corrosion reactions accompanied by the generation of unfavorable by-products. To explore the influence of the IC–Zn gel electrolyte on corrosion reactions, Zn foil was encapsulated in the IC–Zn gel electrolyte and the corrosion products on the surface were detected by XRD (Fig. S8†). As shown in Fig. 2e, the characteristic peaks of $Zn_4SO_4(OH)_6 \cdot xH_2O$ were detected on Zn foil after immersing in $ZnSO_4$ aqueous electrolyte for 5 days. However, the XRD pattern of Zn foil encapsulated in IC–Zn gel electrolyte for 5 days is consistent with that of Zn foil without any impurity peaks. Even if the time of encapsulation in IC–Zn was prolonged to 7 days, no corrosion products were detected. As shown in Fig. 2f and g, the surface of the Zn foil is covered with the insulating corrosion products after the corrosion test for 5 days in 2 M $ZnSO_4$. In contrast, no corrosion product is observed after Zn anode encapsulation with the IC–Zn gel electrolyte for 7 days (Fig. 2h and i). SEM images and the XRD results show that the corrosion reactions are inhibited in the IC–Zn gel electrolyte.

The electrochemical stability window (ESW) of the IC–Zn gel electrolyte and various aqueous electrolytes was measured using linear sweep voltammetry curves. Clearly, the IC–Zn gel electrolyte possesses a wider ESW of 2.7 V in comparison with 2 M $ZnCl_2$ (1.5 V) and 2 M $ZnSO_4$ aqueous electrolyte (2.6 V) (Fig. 3a). The experimental results indicate that the IC–Zn gel electrolyte can effectively inhibit the occurrence of side reactions, such as the hydrogen evolution reaction and oxygen evolution reaction, which can be attributed to the confinement of water molecules in the IC–Zn gel electrolyte limiting the occurrence of corrosion reactions.

The deposition behavior of Zn symmetric cells with different electrolytes was studied by chronoamperometry (CA) under an overpotential of 200 mV. The gradually increasing deposition current (Fig. 3b) is mainly attributed to the continuous growth of Zn with additional surface area, thus leading to the formation of dendrites with expansion of deposition.[19,35] In contrast, the three-dimensional diffusion process allows the stable current density to be reached in only 13 s for the IC–Zn gel electrolyte, which leads to uniform Zn deposition.

Combining with the SEM images, the inhibition of Zn dendrites can be more strongly illustrated. Rapid formation and rampant growth of Zn dendrites were observed in aqueous electrolyte (Fig.S9a and b†). In contrast, no obvious bulge was observed on the zinc surface after cycling in IC–Zn gel electrolyte (Fig. S9c and d†). In aqueous electrolyte, the continuous growth of Zn dendrites intensifies and introduces the risk of short circuits with increasing numbers of cycles (Fig. S10†). Even after 50 h cycling in a symmetrical cell, the electrode surface showed uniform and compact Zn deposition without dendrites (Fig. S11†). This outstanding performance can be attributed to the favorable channels of the IC–Zn gel electrolyte for regulating ion transfer, to achieve uniform Zn plating/stripping.

The resistance of Zn symmetrical cells with IC–Zn-*T* gel electrolytes was evaluated by electrochemical impedance spectra (EIS). Clearly, both IC–Zn-36 gel electrolyte and IC–Zn-48 gel electrolyte exhibited a smaller charge-transfer resistance (Fig. 3c). In contrast, IC–Zn-24 gel electrolyte had a larger charge-transfer resistance due to insufficient cation bridging. The reduction of charge-transfer resistance can be contributed

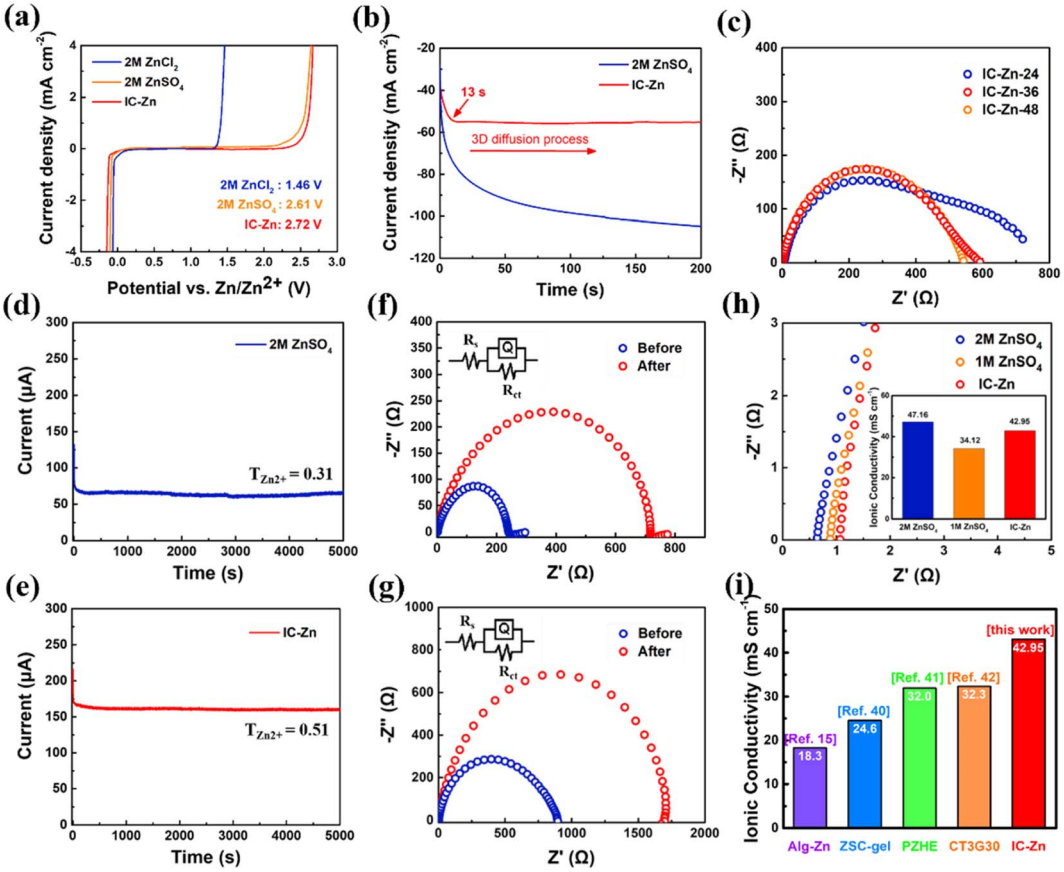

Fig. 3 (a) Electrochemical stability window of different electrolytes. (b) Chronoamperometry curves of Zn symmetric cells with IC–Zn and 2 M $ZnSO_4$ aqueous electrolyte. (c) EIS of IC–Zn-*T* (*T* = 24 h, 36 h and 48 h) gel electrolyte with different times for ion exchange in Zn symmetric cells. *I*–*t* curves of Zn symmetric cells with (d) 2 M $ZnSO_4$ and (e) IC–Zn under an applied potential of 10 mV. EIS spectrum and corresponding equivalent circuit of Zn symmetric cells with (f) 2 M $ZnSO_4$ and (g) IC–Zn before and after polarization. (h) Alternating current impedance spectra of IC–Zn gel electrolyte and aqueous electrolyte, the inset displays the calculated ionic conductivity. (i) Comparison of ionic conductivity between IC–Zn gel electrolyte and other gel electrolytes reported in the literature.[15,40–42]

the high Zn^{2+} content and favorable ion channels in the IC–Zn-36 gel electrolyte. Tensile curves and EIS all indicated that the IC–Zn gel electrolytes reached the stable state after 36 h of ion exchange.

The Zn^{2+} transference number of the IC–Zn gel electrolyte was evaluated using symmetrical cells, at a polarization potential of 10 mV. The corresponding Zn^{2+} transference number ($T_{Zn^{2+}}$) was calculated according to the formula:

$$T_{Zn^{2+}} = \frac{I_S(\Delta V - I_0 R_0)}{I_0(\Delta V - I_S R_S)} \quad (1)$$

where ΔV (mV) is the applied polarization potential, I_0 and I_S (mA) are the current before and after polarization, respectively, and R_0 and R_S (Ω) are the charge-transfer resistance before and after polarization, respectively.[36,37] The Zn^{2+} transference number of 0.51 is much higher than that of 2 M $ZnSO_4$ aqueous electrolyte (0.31) (Fig. 3d–g). Typically, the ion channels of the IC–Zn gel electrolyte enhance the Zn ion flux and Zn ionic mass transfer rate. A high Zn^{2+} transference number can ensure uniform distribution of Zn ions at the electrolyte/anode interface, which is beneficial for uniform Zn deposition during the charging and discharging processes.[37,38]

The ionic conductivity is an extremely important parameter for electrolytes, reflecting the ion transfer ability. The corresponding ion conductivity, σ (mS cm^{-1}), is calculated according to the formula:

$$\sigma = L/RA \quad (2)$$

where *L* (cm) is the distance between the two electrodes (corresponding to the thickness of the gel electrolyte), *R* (Ω) is the bulk resistance and *A* (cm^2) is the contact area of the electrolyte. The thickness of the IC–Zn gel electrolyte (0.46 mm) is the distance *L* (Fig. S12†).[39] As shown in Fig. 3h, the IC–Zn gel electrolyte exhibited an ultra-high ionic conductivity of 42.95 mS cm^{-1}, comparable to that of aqueous electrolyte (2 M $ZnSO_4$ = 47.16 mS cm^{-1}) and even better than those of other gel electrolytes reported previously (Fig. 3i). With the ion channels among the IC–Zn gel electrolyte, the Zn ions are easily transferred so as to enhance ion migration.

As displayed in Fig. 4a and b, Zn‖carbon paper (CP) cells assembled with IC–Zn-36 gel electrolyte exhibited a lower voltage hysteresis (83.3 mV) than for the sample with IC–Zn-24 (100 mV), which suggests a lower energy barrier for the

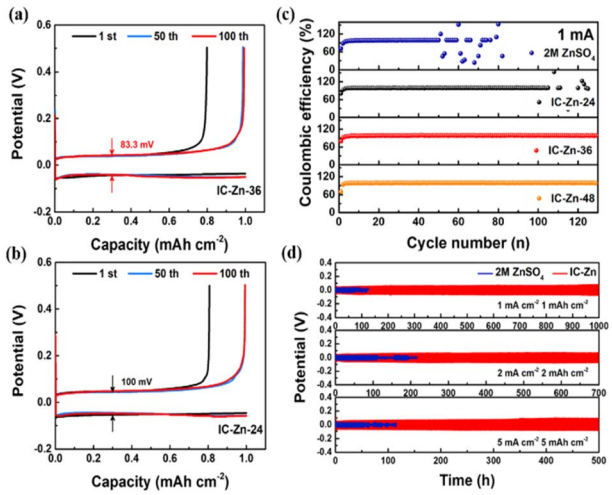

Fig. 4 Voltage–capacity curves of Zn||CP cells with (a) IC–Zn-36 and (b) IC–Zn-24 at 1 mA cm^{-2} for the capacity of 1 mA h cm^{-2}. (c) CE of Zn||CP cells with IC–Zn-*T* and 2 M $ZnSO_4$ aqueous electrolyte. (d) Cycling performance of Zn symmetric cells in 2 M $ZnSO_4$ aqueous electrolyte and IC–Zn gel electrolyte at various current densities and capacities.

favorable plating/stripping process. The overlapped voltage–capacity curves of IC–Zn-36 from the 50th to 100th cycle show the good reversibility. In contrast, the Zn||CP cells with aqueous electrolyte showed abrupt changes after the 50th cycle (Fig. S13†). As shown in Fig. 4c, the coulombic efficiency (CE) of Zn||CP cells with aqueous electrolyte ($ZnSO_4$) showed violent fluctuation after 50 cycles and failed. However, IC–Zn-36 and IC–Zn-48 gel electrolytes all exhibited favorable stability, with an average CE of 98.5% over 120 cycles. In comparison with $ZnSO_4$ electrolyte, the enhanced reversibility of Zn plating/stripping in the IC–Zn gel electrolyte can be attributed to the regulating ability of the ion channels to Zn^{2+} flux, avoiding the formation of "dead" Zn and the growth of Zn dendrites.

Zn symmetric cells with IC–Zn gel electrolyte delivered a stable cycling stability of more than 1000 h at 1 mA cm^{-2} for 1 mA h cm^{-2} (Fig. 4d), which is ten times longer than that in the 2 M $ZnSO_4$ aqueous electrolyte (about 100 h). With increasing current density from 1, 2 to 5 mA cm^{-2}, the batteries with IC–Zn gel electrolyte also exhibited improved cycling stability compared to aqueous electrolyte. In addition, the IC–Zn gel electrolyte also has good stability at low current density, such as 0.2 mA cm^{-2}, and this is maintain for more than 1000 h of cycling (Fig. S14†). In order to investigate the influence of the degree of cation bridging on the cycling stability, the symmetric cell with IC–Zn-24 was tested at 1 mA cm^{-2} for a capacity of 1 mA h cm^{-2} (Fig. S15a†). Compared with IC–Zn, the cycle life was greatly shortened, to less than 150 h, due to the lower concentration of Zn^{2+} and the insufficient degree of cation bridging. In addition, the higher overpotential also showed unfavorable Zn plating/stripping in the IC–Zn-24 gel electrolyte (Fig. S15b†). The outstanding performance of IC–Zn gel electrolyte is derived from ultra-high ionic conductivity and numerous ion channels to accelerate Zn^{2+} transport and regulate Zn^{2+} flux, thus resulting in impressive stability and reversible Zn plating/stripping.

According to the detailed voltage profiles, the polarization of Zn symmetric cells in IC–Zn gel electrolyte increased slowly from 54 to 79 mV over 1000 cycles, which showed a stable Zn plating/stripping process (Fig. S16†). The rate performance of Zn symmetric cells with IC–Zn-*T* gel electrolytes was measured at current densities from 0.5 to 5 mA cm^{-2}. The overpotentials of the Zn symmetric cells with IC–Zn-36 gel electrolyte were lower than those of IC–Zn-24 gel electrolyte, delivering a better rate performance (Fig. S17†). The favorable rate performance of IC–Zn-36 gel electrolyte is attributed to the higher Zn^{2+} content and the facilitation of abundant ion channels for Zn^{2+} transport.

IC–Zn gel electrolyte was assembled with Zn anodes and I_2 cathodes (Fig. S18 and S19†) to form Zn–I_2 batteries and used for further electrochemical testing (Fig. 5). Cyclic voltammetry (CV) with various scan rates was used to characterize the electrochemical reaction kinetics. As shown in Fig. 5a, two distinct anodic peaks and only one cathodic peak were recorded, which is clearly different from the Zn–I_2 battery with aqueous electrolyte (Fig. S20†). The potential difference between the two anodic peaks decreases gradually with increasing scanning rate. To explore the reason for the splitting of the anodic peaks, the battery without I_2 was tested under the same conditions (Fig. S21†). The typical rectangular curve without redox peaks is characteristic of electric double layer capacitance, which demonstrates that both anodic peaks were derived from the oxidation of iodine and its derivatives. Thus, splitting of the anodic peaks was indexed to the $I^-/I_3^-/I_2$ two-step process.[43] Additionally, the two anodic peaks were attributed to the oxidation of I^- and I_3^-, respectively. Moreover, the curves were not distorted with increasing scan rate, indicating high redox reversibility. A good linear relationship between the square root of the scan rate and the redox peak current confirmed the diffusion-controlled redox reaction in the Zn–I_2 batteries with IC–Zn gel electrolyte (Fig. S22†).[44,45]

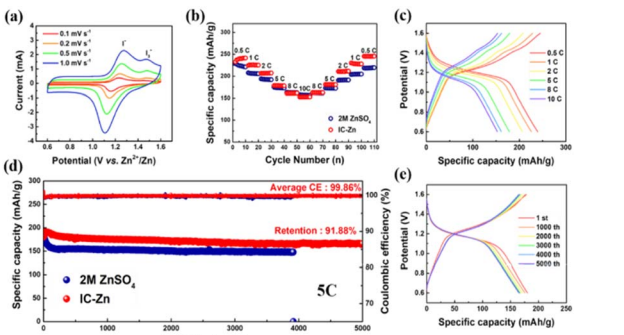

Fig. 5 Comparison of electrochemical performance of different electrolytes in Zn–I_2 batteries. (a) CV curves of Zn–I_2 battery with IC–Zn gel electrolyte under various scanning rates. (b) Rate performance of Zn–I_2 batteries from 0.5C to 10C. (c) Corresponding charge–discharge curves of Zn–I_2 batteries with IC–Zn gel electrolyte. (d) Cycling performance and CE of Zn–I_2 batteries at 5C. (e) Charge–discharge voltage profiles of Zn–I_2 batteries with IC–Zn gel electrolyte at 5C.

The rate performance of Zn–I_2 batteries with different electrolytes was evaluated at 0.5 to 10C. Initially, solid-state Zn–I_2 battery (242 mA h g^{-1}) exhibited a higher specific capacity than aqueous Zn–I_2 battery (223 mA h g^{-1}) at low current densities (Fig. 5b). At the high rate of 10C, both Zn–I_2 batteries with IC–Zn gel electrolyte and with aqueous electrolyte show similar performance. Finally, the Zn–I_2 battery with IC–Zn gel electrolyte (245 mA h g^{-1}) fully recovers its initial specific capacity when returning to the initial rate of 0.5C after 100 cycles. However, it is difficult for the Zn–I_2 battery with aqueous electrolyte to be restored to its initial specific capacity when the rate drops to 0.5C. Clearly, the IC–Zn gel electrolyte shows the better rate performance. In addition, the still obvious charge–discharge plateau at high rates also demonstrates the good rate performance of the IC–Zn gel electrolyte (Fig. 5c).[46,47] The abundant ion channels allow Zn^{2+} to easily reach the electrode surface along a straight line, which facilitates Zn^{2+} transport, thus providing good rate performance.

The self-discharge phenomenon caused by the shuttle effect of I_3^- leads to the capacity loss of Zn–I_2 batteries. In order to explore the influence of the IC–Zn gel electrolyte on the self-discharge behavior of Zn–I_2 batteries, a resting process of 60 h was introduced and the change in open-circuit voltage was recorded. The potential decay of Zn–I_2 battery with IC–Zn gel electrolyte was slowed down compared with that for aqueous electrolyte, which indicates that it shows a positive effect on relieving the self-discharge behavior of the battery (Fig. S23†).

As shown in Fig. 5d, the Zn–I_2 battery assembled with IC–Zn gel electrolyte showed a high specific capacity with a favorable capacity retention (91.9%) and excellent stability after 5000 cycles. The increase of the initial specific capacity may be a short-lived activation process due to the solid–solid interface being a slightly poorer contact than the liquid–solid interface. The stable long-term cycling and extremely high capacity retention are benefited from the regulation of Zn deposition and the promotion of Zn^{2+} transport by the IC–Zn gel electrolyte. In contrast, the specific capacity of the aqueous Zn–I_2 battery dropped rapidly initially and failed within 4000 cycles because of undesirable side reactions and wanton growth of Zn dendrites. Furthermore, the highly overlapping charge–discharge curves also demonstrated the remarkable stability of Zn–I_2 batteries with IC–Zn gel electrolyte during long-term cycling (Fig. 5e).

Conclusions

In conclusion, we have delivered a facile and efficient method to construct a highly conductive multifunctional gel electrolyte with excellent stability *via* the cation bridging effect. The unique zinc ion channels of the IC–Zn gel electrolyte can accelerate ion transport, and exhibit an ion conductivity up to 42.95 mS cm^{-1}, which is almost equivalent to the 2 M $ZnSO_4$ electrolyte. Additionally, the IC–Zn gel electrolyte can also adjust the flux of Zn^{2+} to achieve uniform Zn plating/stripping. As expected, the IC–Zn gel electrolyte exhibited remarkable stability of more than 1000 h in symmetrical cells, which is ten times that with aqueous electrolyte (2 M $ZnSO_4$). Even at a high current density of 5 mA cm^{-2}, the IC–Zn gel electrolyte still showed a lifespan of more than 500 h. Furthermore, Zn–I_2 batteries assembled with IC–Zn exhibited a remarkable stability over 5000 cycles, with an impressive capacity retention (91.9%). Therefore, the rational design of gel electrolytes can effectively prevent the growth of Zn dendrites and facilitate ion transport, thus tremendously extending the lifespan of Zn–I_2 batteries.

Data availability

All data is available in the main text and the ESI.†

Author contributions

Y. Tian and J. Zhang proposed the concept. Y. Tian and S. Ding prepared the materials. Y. Tian, S. Chen and Q. Chen collected relevant data. Y. Tian and J. Zhang co-wrote the manuscript. All authors participated in data analysis and manuscript discussion.

Conflicts of interest

There are no conflicts to declare.

Acknowledgements

This work was financially supported by the National Natural Science Foundation of China (22175108), the Natural Scientific Foundation (ZR2020JQ09 and ZR2022ZD27) and Taishan Scholars Program of Shandong Province, Program for Scientific Research Innovation Team of Young Scholar in Colleges and Universities of Shandong Province (2019KJC025). The authors also acknowledge the assistance of the Analytical Center for Structural Constituent and Physical Property of Core Facilities Sharing Platform, Shandong University.

Notes and references

1 J. Zhou, M. Xie, F. Wu, Y. Mei, Y. Hao, L. Li and R. Chen, *Adv. Mater.*, 2022, 2106897.
2 D. Wang, Q. Li, Y. Zhao, H. Hong, H. Li, Z. Huang, G. Liang, Q. Yang and C. Zhi, *Adv. Energy Mater.*, 2022, 2102707.
3 L. Yan, T. Liu, X. Zeng, L. Sun, X. Meng, M. Ling, M. Fan and T. Ma, *Carbon*, 2022, **187**, 145–152.
4 G. Liang, J. Zhu, B. Yan, Q. Li, A. Chen, Z. Chen, X. Wang, B. Xiong, J. Fan and J. Xu, *Energy Environ. Sci.*, 2022, **15**, 1086–1096.
5 Y. Zou, T. Liu, Q. Du, Y. Li, H. Yi, X. Zhou, Z. Li, L. Gao, L. Zhang and X. Liang, *Nat. Commun.*, 2021, **12**, 1–11.
6 Z. Zhao, J. Zhao, Z. Hu, J. Li, J. Li, Y. Zhang, C. Wang and G. Cui, *Energy Environ. Sci.*, 2019, **12**, 1938–1949.
7 S. Chen, Q. Chen, J. Ma, J. Wang, K. S. Hui and J. Zhang, *Small*, 2022, 2200168.
8 Y. Tian, S. Chen, Y. He, Q. Chen, L. Zhang and J. Zhang, *Nano Research Energy*, 2022, **1**, e9120025.
9 Z. Pei, *Nano Research Energy*, 2022, **1**, e9120023.

10 M. Wang, Y. Meng, K. Li, T. Ahmad, N. Chen, Y. Xu, J. Sun, M. Chuai, X. Zheng and Y. Yuan, *eScience*, 2022, **2**, 509–517.
11 Y. Zhang, Z. Cao, S. Liu, Z. Du, Y. Cui, J. Gu, Y. Shi, B. Li and S. Yang, *Adv. Energy Mater.*, 2022, **12**, 2103979.
12 Z. Guo, L. Fan, C. Zhao, A. Chen, N. Liu, Y. Zhang and N. Zhang, *Adv. Mater.*, 2022, **34**, 2105133.
13 R. Yao, L. Qian, Y. Sui, G. Zhao, R. Guo, S. Hu, P. Liu, H. Zhu, F. Wang and C. Zhi, *Adv. Energy Mater.*, 2022, **12**, 2102780.
14 B. W. Olbasa, C. J. Huang, F. W. Fenta, S. K. Jiang, S. A. Chala, H. C. Tao, Y. Nikodimos, C. C. Wang, H. S. Sheu and Y. W. Yang, *Adv. Funct. Mater.*, 2022, **32**, 2103959.
15 Y. Tang, C. Liu, H. Zhu, X. Xie, J. Gao, C. Deng, M. Han, S. Liang and J. Zhou, *Energy Storage Mater.*, 2020, **27**, 109–116.
16 Y. Shao, J. Zhao, W. Hu, Z. Xia, J. Luo, Y. Zhou, L. Zhang, X. Yang, N. Ma and D. Yang, *Small*, 2022, **18**, 2107163.
17 J. Shi, T. Sun, J. Bao, S. Zheng, H. Du, L. Li, X. Yuan, T. Ma and Z. Tao, *Adv. Funct. Mater.*, 2021, **31**, 2102035.
18 F. Wang, O. Borodin, T. Gao, X. Fan, W. Sun, F. Han, A. Faraone, J. A. Dura, K. Xu and C. Wang, *Nat. Mater.*, 2018, **17**, 543–549.
19 A. Bayaguud, X. Luo, Y. Fu and C. Zhu, *ACS Energy Lett.*, 2020, **5**, 3012–3020.
20 W. Xu, K. Zhao, W. Huo, Y. Wang, G. Yao, X. Gu, H. Cheng, L. Mai, C. Hu and X. Wang, *Nano Energy*, 2019, **62**, 275–281.
21 K. Wu, J. Huang, J. Yi, X. Liu, Y. Liu, Y. Wang, J. Zhang and Y. Xia, *Adv. Energy Mater.*, 2020, **10**, 1903977.
22 P. Burey, B. R. Bhandari, T. Howes and M. J. Gidley, *Crit. Rev. Food Sci. Nutr.*, 2008, **48**, 361–377.
23 J. Necas and L. Bartosikova, *Vet. Med.*, 2013, **58**, 187–205.
24 K. Nishinari and R. Takahashi, *Curr. Opin. Colloid Interface Sci.*, 2003, **8**, 396–400.
25 K. Makino, R. Idenuma, T. Murakami and H. Ohshima, *Colloids Surf., B*, 2001, **20**, 355–359.
26 S. Nanaki, E. Karavas, L. Kalantzi and D. Bikiaris, *Carbohydr. Polym.*, 2010, **79**, 1157–1167.
27 J. Yang, Z. Xu, J. Wang, L. Gai, X. Ji, H. Jiang and L. Liu, *Adv. Funct. Mater.*, 2021, **31**, 2009438.
28 J. Cong, X. Shen, Z. Wen, X. Wang, L. Peng, J. Zeng and J. Zhao, *Energy Storage Mater.*, 2021, **35**, 586–594.
29 L. Zhang, L. Miao, W. Xin, H. Peng, Z. Yan and Z. Zhu, *Energy Storage Mater.*, 2022, **44**, 408–415.
30 C. Huang, X. Zhao, S. Liu, Y. Hao, Q. Tang, A. Hu, Z. Liu and X. Chen, *Adv. Mater.*, 2021, **33**, 2100445.
31 K. Guan, L. Tao, R. Yang, H. Zhang, N. Wang, H. Wan, J. Cui, J. Zhang, H. Wang and H. Wang, *Adv. Energy Mater.*, 2022, **12**, 2103557.
32 P. Wang, S. Liang, C. Chen, X. Xie, J. Chen, Z. Liu, Y. Tang, B. Lu and J. Zhou, *Adv. Mater.*, 2022, **34**, 2202733.
33 J. Prado-Fernández, J. A. Rodrıguez-Vázquez, E. Tojo and J. M. Andrade, *Anal. Chim. Acta*, 2003, **480**, 23–37.
34 J. Wang, Y. Huang, B. Liu, Z. Li, J. Zhang, G. Yang, P. Hiralal, S. Jin and H. Zhou, *Energy Storage Mater.*, 2021, **41**, 599–605.
35 H. Lu, X. Zhang, M. Luo, K. Cao, Y. Lu, B. B. Xu, H. Pan, K. Tao and Y. Jiang, *Adv. Funct. Mater.*, 2021, **31**, 2103514.
36 Y. Cui, Q. Zhao, X. Wu, Z. Wang, R. Qin, Y. Wang, M. Liu, Y. Song, G. Qian and Z. Song, *Energy Storage Mater.*, 2020, **27**, 1–8.
37 L. Suo, Y.-S. Hu, H. Li, M. Armand and L. Chen, *Nat. Commun.*, 2013, **4**, 1–9.
38 H. Jia, M. Qiu, C. Tang, H. Liu, S. Fu and X. Zhang, *EcoMat*, 2022, e12190.
39 H. Yan, S. Li, Y. Nan, S. Yang and B. Li, *Adv. Energy Mater.*, 2021, **11**, 2100186.
40 F. Mo, Z. Chen, G. Liang, D. Wang, Y. Zhao, H. Li, B. Dong and C. Zhi, *Adv. Energy Mater.*, 2020, **10**, 2000035.
41 K. Leng, G. Li, J. Guo, X. Zhang, A. Wang, X. Liu and J. Luo, *Adv. Funct. Mater.*, 2020, **30**, 2001317.
42 M. Chen, J. Chen, W. Zhou, X. Han, Y. Yao and C. P. Wong, *Adv. Mater.*, 2021, **33**, 2007559.
43 Y. Yang, S. Liang, B. Lu and J. Zhou, *Energy Environ. Sci.*, 2022, **15**, 1192–1200.
44 P. Li, X. Li, Y. Guo, C. Li, Y. Hou, H. Cui, R. Zhang, Z. Huang, Y. Zhao and Q. Li, *Adv. Energy Mater.*, 2022, 2103648.
45 Y. He, M. Liu, S. Chen and J. Zhang, *Sci. China: Chem.*, 2022, **65**, 391–398.
46 X. Li, N. Li, Z. Huang, Z. Chen, G. Liang, Q. Yang, M. Li, Y. Zhao, L. Ma and B. Dong, *Adv. Mater.*, 2021, **33**, 2006897.
47 C. Sun, X. Shi, Y. Zhang, J. Liang, J. Qu and C. Lai, *ACS Nano*, 2020, **14**, 1176–1184.